Power Management Strategy for Standalone PV applications with Hybrid Energy Storage System

João Faria, José Pombo, Sílvio Mariano, Maria do Rosário Calado
University of Beira Interior and IT - Instituto de Telecomunicações
Covilhã, Portugal
joaofaria61@gmail.com; jose.pombo@ubi.pt; sm@ubi.pt; rc@ubi.pt

***Abstract*—Hybrid energy storage systems that combine the high density power of the supercapacitors with the high energy density of the Li-ion batteries have been substantially researched, with great interest. This manuscript proposes a new power management strategy implemented using the Rule based controller which considers the state of charge of the Li-ion batteries (SOC). The Li-ion batteries are used to provide a steady and constant power, function of the state of charge (SOC), enabling a higher efficiency and extending batteries lifespan. A typical standalone PV application is used to demonstrate and validate the performance of the proposed power management strategy.**

Keywords— battery management system; DC-DC converters; hybrid energy storage systems; Li-ion batteries; photovoltaic production; supercapacitors.

I. INTRODUCTION

Recent studies have shown a remarkable growth in terms of development and use of new and cleaner energy sources. The use of this type of energy, obtained through direct transformation of natural resources, is currently studied with great interest by the scientific community, due to its complexity, caused by both the different production sources and by its variability and unpredictability. However, this lack of predictability could be compensated by the complementarity between resources or by the introduction of electrical energy storage systems (EESS). The EESS have been recognized as one of the most promising approaches [1], [2]. Nevertheless, these systems suffer from some operational problems, e.g. the performance degradation when subject to high charging/discharging currents, which in turn causes a temperature rise and, consequently, a reduction of its efficiency and lifespan [3]. To mitigate these disadvantages, hybrid energy storage systems (HEES) began to emerge. These systems combine benefits of two or more different technologies. The interconnection of supercapacitors and Li-ion batteries, combining in this manner the high power density of supercapacitors with the high energetic density of the Li-ion Batteries, is the most employed existing topology in HEES. This manuscript presents a real time power management strategy that reduces the dynamic stress and the peak current demand of Li-ion batteries. The control strategy is performed with a Rule Based Controller (RBC), which considers the state of charge of the Li-ion batteries (SOC). Additionally, a typical standalone PV application is used to demonstrate and validate the performance of the proposed power management strategy. With this topology it is possible to transfer the energy from photovoltaic production to the DC bus, and satisfy the load requested by the user at each time instant.

This work is funded by FCT/MEC through national funds and when applicable co-funded by FEDER – PT2020 partnership agreement under the project UID/EEA/50008/2013.

II. SYSTEM DESCRIPTION

A centralized architecture with DC coupling, i.e. in which photovoltaic production unit (programmable source DC SL 500-5.2 and Photovoltaic Power Profile Emulation software) and the hybrid power storage system (HESS) are coupled to a DC-BUS as illustrated in Fig. 1. The power transfer between the HESS and the DC-BUS is performed using two bidirectional non-insulated Buck-Boost DC-DC converters. As for photovoltaic production, the same is extracted to the DC-BUS through a non-insulated Buck-Boost DC-DC converter.

The control unit is Texas Instrument's microcontroller TMS320F28069, a 32 bits fixed point microcontroller used in mathematical tasks with some complexity since it is capable of performing parallel processing. It has a 90MHz Clock frequency with 100kb and 2kb of RAM and ROM memory, respectively and a 256kb flash memory. In addition, it contains 16 PWM channels and 16 ADC channels with 12 bits of resolution and a minimum conversion time of around 333 ns. It also has I2C, CAN and SPI communication capabilities.

Both packs that form the HESS are constituted by a battery management system (BMS) which is based on Intersil's ISL94212 component that enables a maximum of 14 devices in cascade and supports systems up to 168nP (168 cells in series and parallel) as well as extensive monitoring functions. In this work the HESS consists of a Li-ion battery pack (BAT) and a supercapacitors pack (SC) both consisting of 12 cells connected in series.

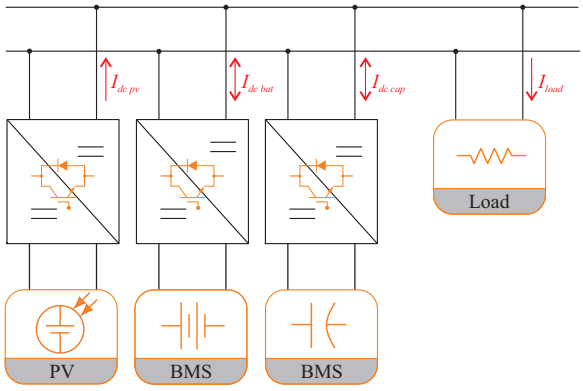

Fig. 1. System scheme description.

978-1-5386-5186-5/18/$31.00 ©2018 IEEE

A. *DC-DC bidirectional converter*

The non-isolated DC-DC bidirectional converter associated with each HESS pack is represented on Fig. 2 [4]. This converter can operate in 4 quadrants and has three possible operating modes, Boost, Buck, Buck-Boost. Various efficiency enhancement modulation strategies have been proposed and investigated in the literature to allow the operation of the converter in soft-switching or hard-switching. A common way to accomplish a modulation strategy with soft-switching is to use an auxiliary circuit including auxiliary switches, inductors and/or capacitors [4], [5]. However, the most common modulation strategy is with hard switching because it has the advantages of being relatively quick and easy to implement, not requiring auxiliary circuits and their control structures are simple. There are two different ways to implement a modulation strategy with hard-switching for each mode of operation, synchronous and asynchronous. As we can see in Tables I and II, in the asynchronous mode only one mosfet is switched, the rest of the driving is done by the free wheel diodes. In the synchronous mode two mosfets are switched in complement. In this way, the drop voltage associated with the diode ceases to exist, and the efficiency is then increased. Therefore, in this manuscript, synchronous switching is used because it guarantees a higher converter efficiency.

TABLE I. BATTERY OR SC DISCHARGE

	Boost		**Buck**		**Buck-Boost**	
	Async	***Sync***	***Async***	***Sync***	***Async***	***Sync***
S1	1	1	PWM	PWM	PWM	PWM
S2	0	0	0	$\overline{PWM}$	0	0
S3	PWM	PWM	0	0	PWM	PWM
S4	0	$\overline{PWM}$	1	1	0	1

TABLE II. BATTERY OR SC CHARGE

	Boost		**Buck**		**Buck-Boost**	
	Async	***Sync***	***Async***	***Sync***	***Async***	***Sync***
S1	0	$\overline{PWM}$	1	1	0	1
S2	PWM	PWM	0	0	PWM	PWM
S3	0	0	0	$\overline{PWM}$	0	0
S4	1	1	PWM	PWM	PWM	PWM

B. *Maximum Power Point Tracking (MPPT)*

In an optimized production of photovoltaic energy is intended to withdraw the maximum of available power, to maximize the energy production at any instant of time, thus increasing the efficiency of the system.

Under uniform irradiation, a photovoltaic panel (PV) must operate at an operation state which corresponds to the maximum available power. This point is called Maximum Power Point (MPP) and depends mainly on the temperature and the solar irradiation. Due to this feature, it becomes necessary to develop a controller that finds this MPP. There are several Maximum Power Point Tracking (MPPT) algorithms, that differ in complexity, speed of convergence, required sensors, cost, efficiency, hardware implementation, popularity, among other aspects. Are example of these the perturb and observe (P&O), incremental conductance, ripple correlation control (RCC), current sweep or fuzzy logic control algorithms, that can be found in the literature [6]–[10].

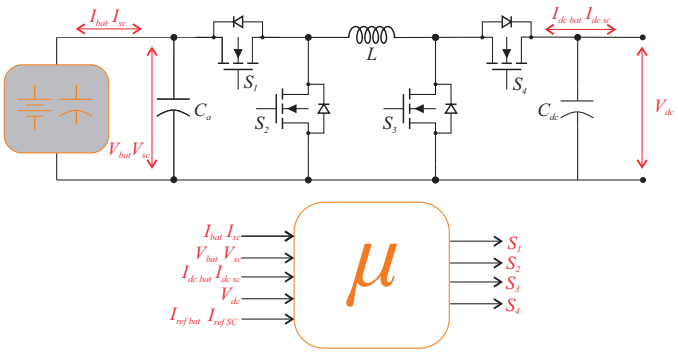

Fig. 2. Implemented Batteries/Supercapacitors power converter.

The implemented algorithm in this manuscript was the perturb and observe (P&O). In Fig. 3 are represented two classical configurations of P&O. In configuration a) the control is done without feedback (open loop), the algorithm consists in perturbing the converter modulation index (duty-cycle), performing afterwards periodic samplings of the current and the voltage from the PV, I_{pv} and V_{pv} respectively [11]. Once known the derivative of the power in relation to the voltage, the control algorithm changes the converter modulation index (duty-cycle) with an adaptive step, in a way that the PV works at the MPP. For configuration b), the control is performed with feedback (closed loop) of the PV voltage, V_{pv}, or current, I_{pv}. The algorithm introduces a perturbation, in the reference. afterwards, the derivative of the power in relation to the voltage is compared and the voltage controller changes the converter modulation index so that the converter works at maximum power point.

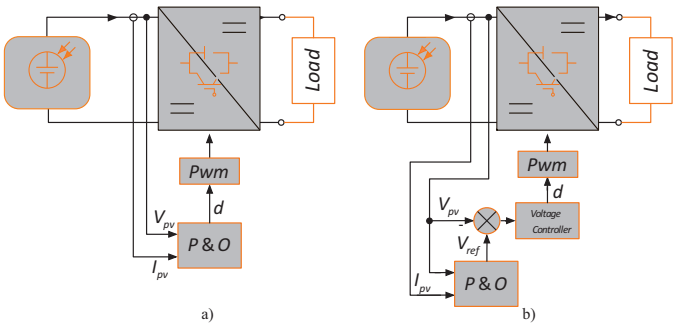

Fig. 3. P&O Configurations: a) open loop; b) closed loop.

In order to maximize the energy extracted from the PV, is required a power processing unit (DC-DC converter), capable of self-tuning, based on the information of the MPPT. The Fig. 4 shows the non-isolated Buck-Boost converter responsible for this maximization at any instant of time. The control is performed without feedback (open loop).

C. *Batteries and Super-Capacitors*

The necessity of connecting cells in series to obtain the required voltage levels, and the fact that all cells have intrinsic and extrinsic differences, results in a lack of uniformity that reduces usable capacity, lifespan, and performance [12].

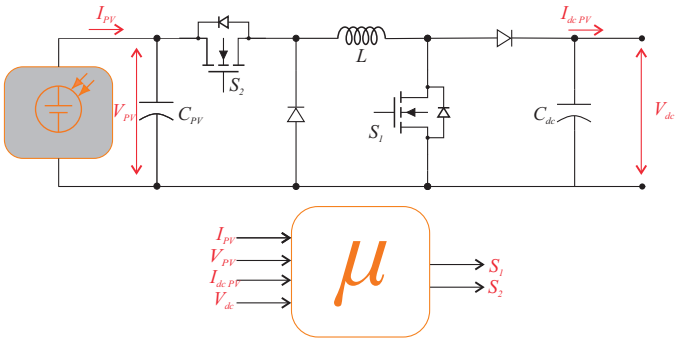

Fig. 4. Implemented PV power converter.

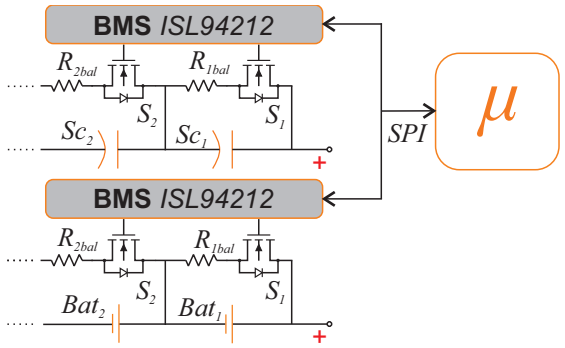

Fig. 5. Implemented BMS Arquitecture.

These cells intrinsic differences are mainly due to small variations in the construction process, different capacities, volume, internal impedance and different rates of self-discharge, which with the increasing number of charging and discharging cycles are getting worse.

Due to these facts, it is required to monitor the battery pack through a Battery Management Systems (BMS). The BMS functions consists in monitoring and controlling some parameters (e.g., voltage, current, temperature, etc.) to provide a safe, efficient and reliable use, thermal stability, usable capacity maximization as well as a longer battery pack lifespan. In terms of the BMS architectures these can be classified as centralized or decentralized, and the structure (electrical circuit of both BMS and battery pack) can be classified as static or dynamic. The main advantages and disadvantages of each architecture and structure can be found in [13].

One of the main functions of BMS is to balance the cells that integrate the battery pack to maximize the usable capacity at each charge and discharge cycle. In addition to maximize the usable capacity, balancing avoids overcharging and over discharging problems that result in a reduced lifespan of the cells and the pack, in extreme cases it results in complete destruction of these, with the possibility of explosion [13].

Fig. 5 illustrates the implemented BMS, which is a centralized architecture with a balancing methodology designated as switched shunt resistor [12]. It is a passive methodology that is highly used in the automobile industry given its simplicity, cost, efficiency, volume, weight, robustness and reliability [12]. It is based in a cell bypass process, in which each cell that forms the pack is associated with a balancing resistor (R_{bal}) and a switch controlled by the BMS. The cells are balanced by discharging when the battery is not being used, or by providing an alternative path for the current to flow while it is being charged until all the cells have reached the same voltage or SOC. The main disadvantage of this method is that the energy is dissipated in a form of heat. Both BMS units communicate with the control unit through Serial-Peripheral-Interface (SPI) protocol.

Fig. 6 shows the developed and implemented hardware, i.e., the control unit (TMS320F28069), the three non-isolated DC-DC converters and the two BMS associated to the HESS.

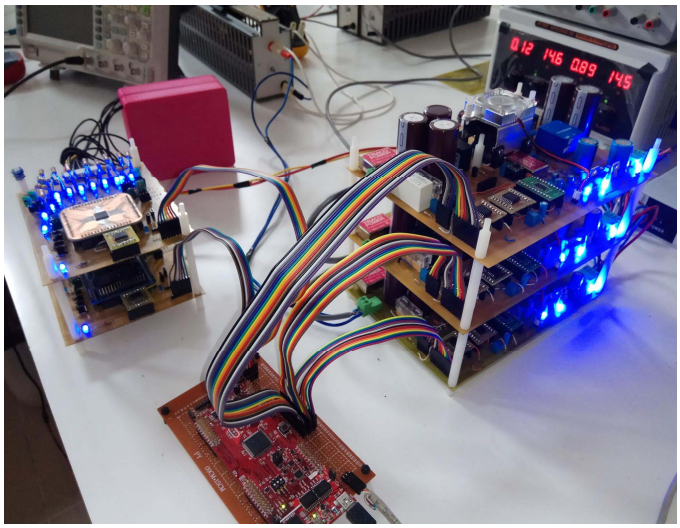

Fig. 6. Developed and implemented hardware.

III. POWER MANAGEMENT STRATEGY

A. *Management Strategy and Control Scheme*

The power management strategy consists in solving in real time the dynamic power flow problem after the power conversion (DC-BUS), synthetized by (1):

$$P_{dc\,pv} + P_{dc\,bat} + P_{dc\,SC} - P_{load} = 0, \quad (1)$$

where $P_{dc\,pv}$ is the power generation of the PV, $P_{dc\,bat}$ is the power flow of the Li-ion battery, $P_{dc\,SC}$ is the power flow of the SC and P_{load} is the power demanded by the load.

In this manuscript the power sharing between the Li-ion batteries and the SC was implemented using the Rule Based Controller. The RBC is developed and expressed in the form of dead-zone function [2], [14]. In the implemented RBC, during the charging period and if the charging current exceeds the maximum allowed battery charging current ($I_{\max\,bat}$), the remaining current is shared with the SC. In the discharge case, if the battery current demand is within the threshold $I_{dis\max\,bat}$, the batteries are the only source to supply the load. However, if the battery current demand exceeds the maximum allowed discharging current ($I_{dis\max\,bat}$), the remaining current is

supplied by the SC. The capacity of the Li-ion cells was taken into account to determine the maximum battery charging current ($I_{\max\ bat}$) and the maximum discharging current ($I_{dis\max\ bat}$).

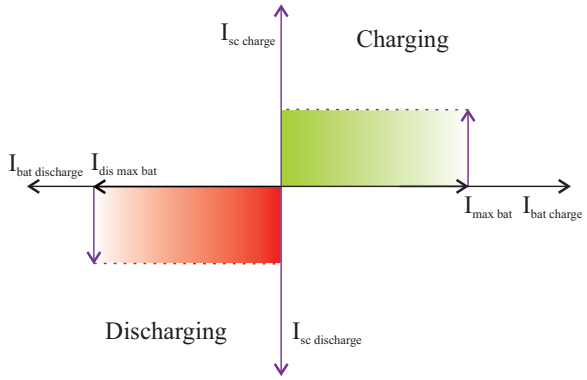

Fig. 7. Implemented Rule Based Controller.

The balancing algorithm acts over the cells with higher voltage or higher SOC, until all the cells in the pack have the same voltage or SOC. The implemented algorithm is executed in the inactive periods of the pack ($I_{bat}=0$ and $I_{sc}=0$) or in the pack charging periods ($I_{bat}>0$ and $I_{sc}>0$). The decision regarding which cells should be balanced depends on the voltage of each cell, given by the following equation:

$$V_{i,k} = \xi_k + 0.01 \qquad (2)$$

where $V_{i,k}$ is the voltage of the cell *i* at the instant of time *k* and ξ_k is the mean cell voltages at the instant of time *k*.

The control can be operated in two different modes, closed-loop current control or closed-loop voltage control, as shown in Fig. 8. Both control schemes are similar and composed by three Proportional Integral controllers with anti-Wind-Up mechanism (PI-awu). In the closed-loop voltage control, the reference is the value selected for the DC bus (V_{dc}). The current references are generated by the implemented RBC, which output control signal is the input of the two controllers (PI-awu) with current feedback. These controllers act by adjusting the modulation index to control the output current of each converter with the aim of minimize the errors between the reference currents ($I_{bat\ ref}$ and $I_{sc\ ref}$) and the DC bus currents ($I_{dc\ bat}$ and $I_{dc\ sc}$). The closed-loop current controller is similar to the voltage closed-loop controller. However, the only difference is the reference signal, which is the load current (I_{dc}).

To determine the optimal parameters of the controllers (PI-awu), for both control strategies, the algorithm Particle Swarm Optimization (PSO) was used [15]. The objective function (OF) is given by (2), for the closed-loop voltage control, that consists in the Integral of the Absolute Error (IAE) between the reference currents ($I_{Bat\ ref}$ and $I_{SC\ ref}$) and the output currents of each converter ($I_{dc\ bat}$ and $I_{dc\ sc}$) with the absolute error between the voltage reference ($V_{dc\ ref}$) and the DC-BUS voltage. The OF for the closed-loop current control is given by (3), similar to the previous OF but with the absolute error between the current reference ($V_{dc\ ref}$) and the load current.

$$OF = \int_{t_0}^{t_0+t} \left|I_{bat\ ref} - I_{dc\ bat}\right| + \left|I_{sc\ ref} - I_{dc\ sc}\right| + \left|V_{dc\ ref} - V_{dc}\right| dt \qquad (2)$$

$$OF = \int_{t_0}^{t_0+t} \left|I_{bat\ ref} - I_{dc\ bat}\right| + \left|I_{sc\ ref} - I_{dc\ sc}\right| + \left|I_{dc\ ref} - I_{dc}\right| dt \qquad (3)$$

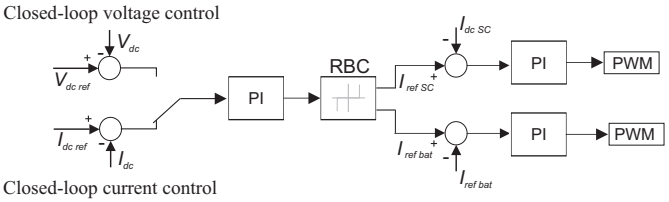

Fig. 8. Control Strategies.

IV. Simulation And Experimental Results

To evaluate the performance of the power management strategy, the system of Fig. 1 was implemented and simulations were performed for both control schemes, in Simulink software, from MathWorks®. The system has a PV, characterized with a power of 200 Wp, under a uniform irradiation of 1000 W/m^2. The HESS system is composed by 12 Li-ion battery cells, connected in series, with a nominal capacity of 2 Ah and 12 supercapacitors, connected in series, with a nominal capacitance of 5 F. It was assumed that the initial SOC for both technologies i.e., for the Li-ion battery cells and supercapacitors, was 50%.

A. *Simulation results for the closed-loop voltage control*

In this case study, the DC-BUS voltage reference was set at 60V and the system was subjected to various load disturbances. Fig. 9a shows the evolution of the currents, where we can verify the excellent performance of the controllers and the power management strategy implemented. From Fig. 9a, we can conclude that: i) in several situations, for example in the time period between 8 and 10 seconds, $P_{dc\ pv} > P_{load}$ and the charging current exceeds the maximum value allowed for the battery charging current ($I_{\max\ bat}$) and, consequently, the remaining current is shared with the SC; ii) in the time period between 5 and 7 seconds, the $P_{dc\ pv} < P_{load}$ and the battery current demand exceeds the maximum allowed discharging current ($I_{dis\max\ bat}$) and the remaining current is supplied by the SC; iii) in the time period between 1 and 3 seconds, $P_{dc\ pv} < P_{load}$ and the current demand not exceeds the maximum allowed and, consequently, the Li-ion batteries are the only source to supply the load; iv) in the time period between 3 and 5 seconds, $P_{dc\ pv} \approx P_{load}$ and PV is the only source to supply the load; v) in all the transient response of the system the supercapacitors are requested to minimize the dynamic stress and the peak current demand of the Li-ion batteries.

Fig. 9b shows the evolution of the system voltages, where we can verify that: i) the MPPT algorithm reaches the maximum

power point in less than 1 second; ii) after reaching the maximum power point, the MPPT algorithm oscillates around this value; iii) the excellent response of the controllers following the voltage reference, which in this case was 60 V.

Fig. 10a illustrates the dynamic power flow of the HESS and PV, after the power conversion (DC-BUS), where we can verify, once again, the excellent performance of the implemented controllers. Fig. 10b illustrates the evolution of the load power flow.

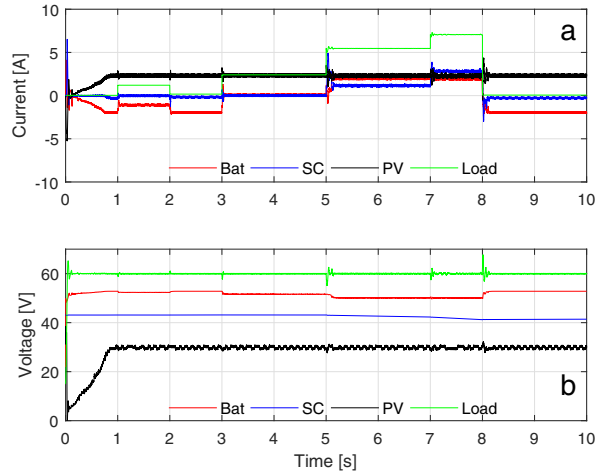

Fig. 9. System with closed-loop voltage control − currents and voltages

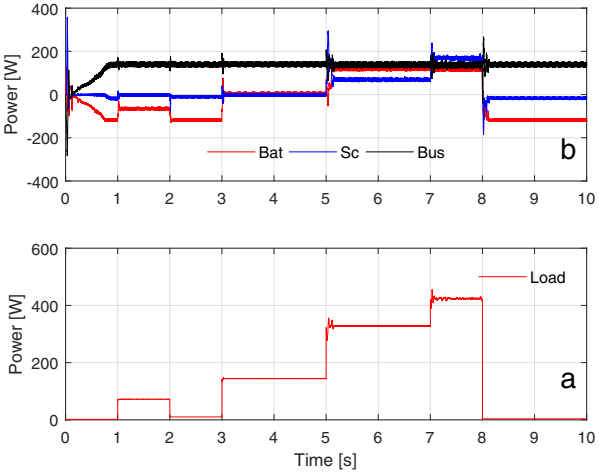

Fig. 10. System with closed-loop voltage control − power flow

B. *Simulation results for the closed-loop current control*

In this case study, the system was subjected to several disturbances in the reference DC-BUS voltage. Fig. 11a presents the evolution of the currents. By analyzing the figure, we can conclude that: i) in this control scheme, the transient response of the system presents much more overshoot; ii) however, in all the transient responses of the system the supercapacitors are requested to minimize the dynamic stress and the peak current demand of the Li-ion batteries; iii) although both controls schemes are similar, this type of disturbance is more difficult for the system because the converters have to change their operation mode i.e., in the time period between 8 and 10 seconds and between 3 and 5 seconds, the converter responsible for the MPPT had to change its operation mode to Buck because the PV voltage is less than the DC-BUS voltage; iv) the considerations made for the previous case study, concerning the power sharing between the Li-ion batteries and the SC, are similar.

Fig. 10b shows the evolution of the system voltages, where we can verify that: i) as in the previous case study, the MPPT algorithm reaches the maximum power point in less than 1 second; ii) when the converter had to change its operation mode, the power extraction from the PV is misrepresented; iii) the excellent response of the controllers in following the current reference.

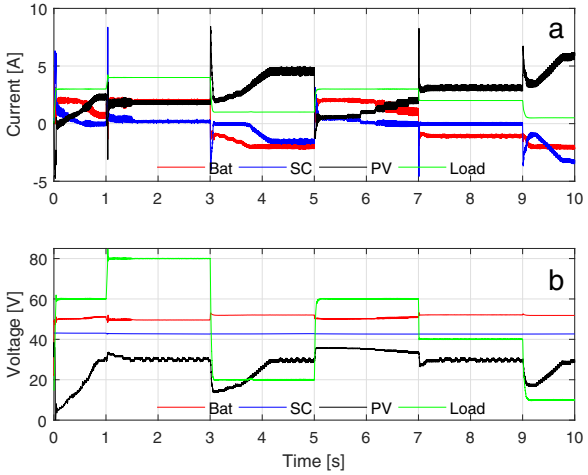

Fig. 11. System with closed-loop current control − currents and voltages

C. *Experimental results*

To validate the proposed and simulated methodology, the closed-loop current control was experimentally performed. The control unit (controllers and the power management strategy) was implemented in the TMS320F28069 microcontroller from

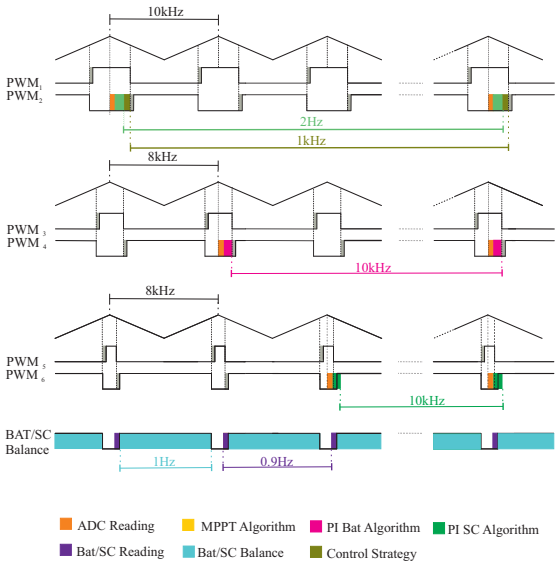

Fig. 12. Time sequence of the proposed algorithm as a function of the CPU usage.

Texas Instruments and was written in C language in the Code Composer Studio ® software.

Fig 12 illustrates the time sequence of the proposed control scheme as a function of the CPU usage. The associated routines in each converter are triggered by its respective EPWM timer module and configured for a frequency that corresponds to the switching frequency of the DC-DC converter. In the converter associated to the photovoltaic production (PWM_1-PWM_2), the ADC Reading is triggered with a frequency of 10kHz. This routine is responsible for the calculation of the photovoltaic panel average values of current (I_{av_pv}) and voltage (V_{av_pv}), which will be used in the MPPT routine, executed with a frequency of 2Hz. In the batteries Li-ion pack converter (PWM_3-PWM_6) and in the supercapacitors pack converter (PWM_7-PWM_{10}), the ADC Reading routine is executed with a frequency of 8kHz and the PI Bat algorithm routine and PI SC algorithm routine are executed with a frequency of 10kHz. The proposed control strategy routine is executed with a frequency of 1Khz. Since the cell balancing influences the voltage readings, between the duration of the balancing process (defined as 1 minute) and the cell voltages acquisition, a time lag of 5 seconds was added. Thus, cell voltages acquisition is performed at a frequency defined by $1/(time\_bal+5)$.

In Fig. 13 is illustrated the real system in operation, with an emphasis on the photovoltaic power profile emulation software (Magna Power®) and on the voltages of the system. The MPPT real implementation results are similar to the ones achieved in the simulation. The MPP is reached in about 1 second and the DC-DC converter functioning point oscillates around it, with adaptive step. In the oscilloscope print screen is showed a situation where the DC bus (line in magenta) is set at 85V. The batteries (line in yellow) are charging with a constant current of 1A and a voltage of 38V, the super-capacitors (line in blue) are resting because the charging current of the batteries does not exceeds 2A.

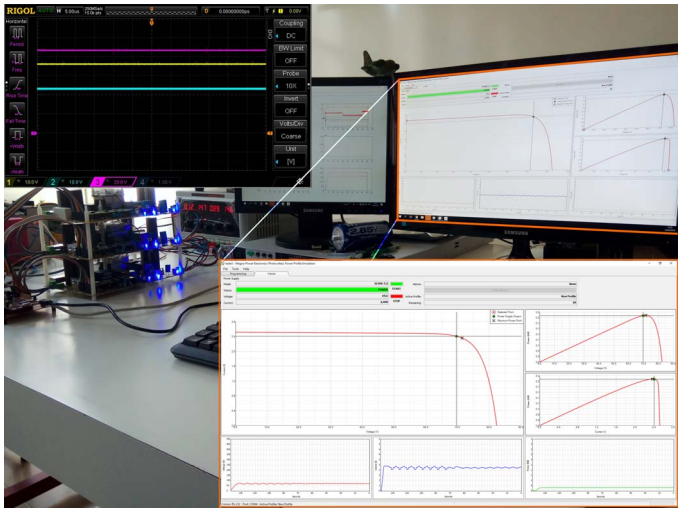

Fig. 13. Real system assembly in functioning

V. CONCLUSIONS

A new power management system for PV standalone applications with hybrid energy storage system is proposed in this manuscript. This proposed management system allows the best performance of the system and increase lifespan of the batteries. Simulation and experimental results shown that this power management system is highly efficient, for solar standalone and grid-tied applications. This is due to the system improvement in PV power extraction allied with the batteries lifespan increasing.

REFERENCES

[1] W. Jing, C. H. Lai, W. S. H. Wong, and M. L. D. Wong, "Dynamic power allocation of battery-supercapacitor hybrid energy storage for standalone PV microgrid applications," *Sustain. Energy Technol. Assessments*, vol. 22, pp. 55–64, 2017.

[2] L. W. Chong, Y. W. Wong, R. K. Rajkumar, and D. Isa, "An optimal control strategy for standalone PV system with Battery-Supercapacitor Hybrid Energy Storage System," *J. Power Sources*, vol. 331, pp. 553–565, 2016.

[3] K. Uddin, A. D. Moore, A. Barai, and J. Marco, "The effects of high frequency current ripple on electric vehicle battery performance," *Appl. Energy*, vol. 178, pp. 142–154, Sep. 2016.

[4] S. Waffler and J. W. Kolar, "A Novel Low-Loss Modulation Strategy for High-Power Bidirectional Buck + Boost Converters," *IEEE Trans. Power Electron.*, vol. 24, no. 6, pp. 1589–1599, 2009.

[5] K. Bin Liu, C. Y. Liu, Y. H. Liu, Y. C. Chien, B. S. Wang, and Y. S. Wong, "Analysis and controller design of a universal bidirectional DC-DC converter," *Energies*, vol. 9, no. 7, 2016.

[6] T. Esram and P. L. Chapman, "Comparison of Photovoltaic Array Maximum Power Point Tracking Techniques," *IEEE Trans. Energy Convers.*, vol. 22, no. 2, pp. 439–449, Jun. 2007.

[7] N. Onat, "Recent Developments in Maximum Power Point Tracking Technologies for Photovoltaic Systems," *Int. J. Photoenergy*, vol. 2010, pp. 1–11, 2010.

[8] A. Anurag, S. Bal, S. Sourav, and M. Nanda, "A review of maximum power-point tracking techniques for photovoltaic systems," *Int. J. Sustain. Energy*, no. September, pp. 1–24, May 2014.

[9] A. N. A. Ali, M. H. Saied, M. Z. Mostafa, T. M. Abdel- Moneim, and T. M. A.-M. Ali Nasr Allah Ali, Mohamed H. Saied, M. Z. Mostafa, "A Survey of Maximum PPT techniques of PV Systems," *Optim. Electr. Electron. Equip.*, p. 1097,1102, May 2012.

[10] B. Subudhi and R. Pradhan, "A comparative study on maximum power point tracking techniques for photovoltaic power systems," *Sustain. Energy, IEEE …*, vol. 4, no. 1, pp. 89–98, 2013.

[11] T. Logeswaran and A. SenthilKumar, "A Review of Maximum Power Point Tracking Algorithms for Photovoltaic Systems under Uniform and Non-uniform Irradiances," *Energy Procedia*, vol. 54, pp. 228–235, Jan. 2014.

[12] R. Velho, M. Beirão, M. Calado, J. Pombo, J. Fermeiro, and S. Mariano, "Management System for Large Li-Ion Battery Packs with a New Adaptive Multistage Charging Method," *Energies*, vol. 10, no. 12, p. 605, May 2017.

[13] S. Steinhorst *et al.*, "Distributed reconfigurable Battery System Management Architectures," *Proc. Asia South Pacific Des. Autom.* Conf. ASP-DAC, vol. 25-28-NaN-2016, pp. 429–434, 2016.

[14] Y. Zhang, Z. Jiang, and X. Yu, "Control Strategies for Battery/Supercapacitor Hybrid Energy Storage Systems," in 2008 IEEE Energy 2030 Conference, 2008, pp. 1–6.

[15] J. B. L. Fermeiro, J. A. N. Pombo, M. R. A. Calado, and S. J. P. S. Mariano, "A new controller for DC-DC converters based on particle swarm optimization," Appl. Soft Comput., vol. 52, pp. 418–434, Mar. 2017.